Topologically twisted index in the 't Hooft limit and the dual AdS_4 black hole entropy

Leopoldo A. Pando Zayas[1,2,*] and Yu Xin[1,†]

[1]*Leinweber Center for Theoretical Physics, Randall Laboratory of Physics The University of Michigan, Ann Arbor, Michigan 48109, USA*

[2]*The Abdus Salam International Centre for Theoretical Physics, Strada Costiera 11, 34014 Trieste, Italy*

(Received 20 October 2019; published 19 December 2019)

We study the topologically twisted index of $\mathcal{N}=6$ supersymmetric Chern-Simons matter theory with $U(N)_k \times U(N)_{-k}$ gauge group in the 't Hooft limit, that is, for $N, k \to \infty$ with $\lambda = N/k$ fixed. In the regime where λ is fixed and large we find an analytical expression for the leading order term of the index. The leading term of the index matches precisely the Bekenstein-Hawking entropy of the dual asymptotically AdS_4 magnetically charged black holes embedded in IIA supergrvity on $AdS_4 \times \mathbb{CP}^3$, after a standard Legendre transformation. We numerically explore the genus expansion of the topologically twisteed index beyond the leading order, focusing on the genus one contribution, that is, N^0. We find qualitative agreement with the topological expansion of the free energy on S^3 at genus one. Our logarithmic in λ term constitutes a prediction for the one-loop effective action on the IIA supergravity side.

DOI: 10.1103/PhysRevD.100.126019

I. INTRODUCTION

One of the best established pairs of the AdS/CFT correspondence is the duality between Chern-Simons matter theory with gauge group $U(N)_k \times U(N)_{-k}$ and string theory. In the large N limit there are, in fact, two distinctive regimes: for large N and fixed k the dual gravity is found in M-theory while in the 't Hooft limit, that is, large N and k with $\lambda = N/k$ fixed, the gravity theory is low energy string theory on $AdS_4 \times \mathbb{CP}^3$ [1].

The difference between the M-theory limit and the IIA limit has been one of the most interesting aspects of this duality since its very early inception. In particular the $N^{3/2}$ versus the N^2 growth in the number of the degrees of freedom has been one of the most enigmatic problems that the correspondence has elucidated [2]. The clarification was made manifest by studying the free energy on S^3 which cleanly captures the two behaviors [2]; such analysis has also shed light on various nonperturbative aspects [3]. It is thus expected that other observables related to counting of degrees of freedom should follow and enrich this dichotomy. One such observable is the topologically twisted index [4–10].

There has recently been a remarkable development in our understanding of the microscopic origin of the entropy for asymptotically AdS_4 black holes precisely via studies of the topologically twisted index [11–16], for recent reviews of these developments, including full lists of references, see [17,18]. Most of the discussion thus far has been focused in the M-theory regime where the leading term is of the order $N^{3/2}$ or N^3; in this manuscript we focus on the IIA regime with N^2 growth. Explorations beyond the leading order have also proven fruitful. In particular, the sub-leading logarithmic in N corrections for the Aharony-Bergman-Jafferis-Maldacena (ABJM) theory and the Chern-Simons matter theory dual to massive IIA have been discussed in [19,20], respectively. The more subtle issue of matching with the one-loop quantum supergravity has been achieved in [21] after various discussions [19,22] (see also [23]). More recently, subleading matching in the context of asymptotically AdS_4 black holes obtained from M5 branes wrapping hyperbolic three-manifolds was demonstrated in [24,25]. The 3d-3d correspondence allows us to evaluate the large N partition functions using Chern-Simons topological invariants, thus providing analytic control over the results which is not the case in the theories related to M2 branes.

In this manuscript we extend the analysis of the topologically twisted index of ABJM theory to the 't Hooft limit: $N, k \to \infty$ holding $\lambda = N/k$ fixed. We then compare with the supergravity Bekenstein-Hawking entropy which is valid for large values of λ. The leading in N term for the topologically twisted index equals

*lpandoz@umich.edu
†yxinee@umich.edu

$$\mathrm{Re}\log Z = -\frac{1}{3}\frac{N^2}{\sqrt{\lambda}}\sqrt{2\Delta_1\Delta_2\Delta_3\Delta_4}\sum_a \frac{n_a}{\Delta_a}. \quad (1.1)$$

The above expression precisely reproduces, after a Legendre transformation, the entropy of the dual magnetically charged black holes asymptotically to $AdS_4 \times \mathbb{CP}^3$. We emphasize that the matching takes place for large values of λ and further demonstrate numerically that the fitting improves for large values of λ.

We also study the first subleading in N term, namely, the genus one in the topological expansion which is proportional to N^0. We confirm that this term contains a dependence of the type $\sqrt{\lambda}$, as expected from the form of the free energy of ABJM on S^3. In the special case when all the fugacities take the same value $\Delta_a = \pi/2$ we find a term of the form

$$\frac{2\pi}{3}\sqrt{2\lambda}. \quad (1.2)$$

The analogous term in the expansion of the free energy on S^3 was interpreted as a nonperturbative instanton effect in IIA string theory [3]. At the same level in the genus expansion, N^0, we also find a logarithmic in λ term whose coefficient is estimated to be $-7/6$. It would be quite interesting to understand this contribution from the point of view of the supergravity one-loop effective action.

The rest of the manuscript is organized as follows. We briefly review the topologically twisted index of ABJM theory in Sec. II. Section III contains various aspects of the evaluation of the topologically twisted index in the 't Hooft limit, we consider the behavior of the eigenvalues in great detail and evaluate the leading part of the index using analytic techniques and present various numerical results for the subleading behavior. We work in details the special case $\Delta_a = \pi/2$, because this choice has a number of simplifying properties. We also consider more generic values of Δ_a. In Sec. IV we briefly discuss the gravity side. We conclude in Sec. V. We relegate a number of more technical issues to two appendices where we discuss, in particular, aspects of our numerical algorithm and details of the supergravity solution.

II. REVIEW OF THE TOPOLOGICALLY TWISTED INDEX OF ABJM THEORY

We follow the works of [4,6,8,9] in general and stay particularly close to the presentation by Benini, Hristov and Zaffaroni in [11]. The outcome of the localization process is an expression for the topologically twisted index for ABJM which we aim to numerically explore in the 't Hooft limit.

Let us briefly recall the key ingredients as a way to also explain the notation. One considers the field theory on $S^2 \times S^1$ with a background field A^R. For ABJM one includes a set of flavor symmetries characterized by Cartan-valued magnetic background flavor symmetry $\frac{1}{2\pi}\int_{S^2} F^f = \vec{n}$. With these flavor symmetries one associates fugacities according to $y = e^{i(A_t^f + i\beta\sigma^f)}$; a similar expression holds for the dynamical fields $x = e^{i(A_t + i\beta\sigma)}$ where the constant potential A_t^f is a flat connection for the flavor symmetry and σ^f is a real mass for the three-dimensional field theory.

For a generic 3d $\mathcal{N} = 2$ theory the topologically twisted index takes the form

$$Z(\vec{n}, y) = \frac{1}{|W|}\sum_{m\in\Gamma_{\mathfrak{h}}}\oint_{\mathcal{C}} Z_{\mathrm{int}}(x, y; m, \vec{n}). \quad (2.1)$$

The sum is over all the magnetic fluxes m in the coroot lattice $\Gamma_{\mathfrak{h}}$ of the gauge group and the integration over the contour $\mathcal{C}$. In localization, the building blocks of Z_{int} are obtained from the classical action and the one-loop evaluation of determinants resulting from quantum fluctuations around the localization locus. A chiral multiplet contributes a one-loop factor of the form

$$Z^{\mathrm{chiral}}_{1-\mathrm{loop}} = \prod_{\rho\in\mathcal{R}}\left(\frac{x^{\rho/2}y^{\rho_f/2}}{1 - x^{\rho}y^{\rho_f}}\right)^{\rho(m)+\rho_f(n)-q+1}, \quad (2.2)$$

where $\mathcal{R}$ is the representation of the gauge group G, ρ denotes the corresponding weights of the representation $\mathcal{R}$, q denotes the R-charge of the field and ρ_f denotes the weights of the multiplet under the flavor symmetry. The vector multiplet contributes the following product of integrals

$$Z^{\mathrm{gauge}}_{1-\mathrm{loop}} = \prod_{\alpha\in G}(1 - x^{\alpha})(idu)^r, \quad (2.3)$$

where r is the rank of the gauge group and α denotes roots of G. We also use $u = A_t + i\beta\sigma$ which lives on the complexified Cartan subalgebra related to $x = e^{iu}$.

The only classical contribution in the ABJM case comes from the Chern-Simons term $Z^{\mathrm{CS}}_{\mathrm{class}} = x^{km}$, where k is the Chern-Simons level and m is a dynamical magnetic flux characterizing the localization locus and living in the coroot lattice $\Gamma_{\mathfrak{h}}$. These are the key ingredients of the construction but for a more detailed description we refer the reader to the original treatment in [11].

In the appropriate basis for the Cartan of global symmetries one has flavor symmetries $J_{1,2,3}$ and there is an additional R-symmetry J_4. One denotes $n_{1,2,3}$ the fluxes and by $y_{1,2,3}$ the fugacities associated to $J_{1,2,3}$. To make expressions symmetric it is convenient to introduce also n_4 and y_4 such that

$$\sum_{a=1}^{4} n_a = 2, \qquad \prod_{a=1}^{4} y_a = 1. \quad (2.4)$$

The topologically twisted index for ABJM takes the form [11]:

$$Z = \frac{1}{(N!)^2}\int_{\mathcal{C}}\prod_{i=1}^{N}\frac{dx_i}{2\pi i x_i}\frac{d\tilde{x}_i}{2\pi i\tilde{x}_i}\prod_{i\neq j}^{N}\left(1-\frac{x_i}{x_j}\right)\left(1-\frac{\tilde{x}_i}{\tilde{x}_j}\right)$$
$$\times\prod_{i,j=1}^{N}\prod_{a=1,2}\left(\frac{\sqrt{\frac{x_i}{\tilde{x}_j}}y_a}{1-\frac{x_i}{\tilde{x}_j}y_a}\right)^{1-n_a}\prod_{b=3,4}\left(\frac{\sqrt{\frac{\tilde{x}_j}{x_i}}y_b}{1-\frac{\tilde{x}_j}{x_i}y_b}\right)^{1-n_b}$$
$$\times\prod_{i=1}^{N}\frac{1}{e^{iB_i}-1}\prod_{i=j}^{N}\frac{1}{e^{i\tilde{B}_j}-1}. \tag{2.5}$$

The contour of integration $\mathcal{C}$ follows the Jeffrey-Kirwan prescription and simply picks up the poles in the last line of Eq. (2.5) which are determined by the following "Bethe Ansatz equations"

$$e^{iB_i} = x_i^k\prod_{j=1}^{N}\frac{(1-y_3\frac{\tilde{x}_j}{x_i})(1-y_4\frac{\tilde{x}_j}{x_i})}{(1-y_1^{-1}\frac{\tilde{x}_j}{x_i})(1-y_2^{-1}\frac{\tilde{x}_j}{x_i})} = 1, \tag{2.6}$$

and

$$e^{i\tilde{B}_j} = \tilde{x}_j^k\prod_{j=1}^{N}\frac{(1-y_3\frac{\tilde{x}_j}{x_i})(1-y_4\frac{\tilde{x}_j}{x_i})}{(1-y_1^{-1}\frac{\tilde{x}_j}{x_i})(1-y_2^{-1}\frac{\tilde{x}_j}{x_i})} = 1. \tag{2.7}$$

Once the solutions to these BAE are known, the final form of the topologically twisted index for ABJM is

$$Z(y_a,n_a) = \prod_{a=1}^{4}y_a^{-\frac{1}{2}N^2n_a}\sum_{I\in\mathrm{BAE}}\frac{1}{\det\mathbb{B}}\times\frac{\prod_{i=1}^{N}x_i^N\tilde{x}_i^N\prod_{i\neq j}(1-\frac{x_i}{x_j})(1-\frac{\tilde{x}_i}{\tilde{x}_j})}{\prod_{i,j=1}^{N}\prod_{a=1,2}(\tilde{x}_j-y_ax_i)^{1-n_a}\prod_{a=3,4}(x_i-y_a\tilde{x}_j)^{1-n_a}}, \tag{2.8}$$

where y_a are the corresponding fugacities. The summation is over all solutions I of the "Bethe Ansatz equations" (BAE) $e^{iB_i} = e^{i\tilde{B}_j} = 1$ modulo permutations. The two sets of variables $\{x_i\}$ and $\{\tilde{x}_j\}$ arise from the $U(N)_k\times U(N)_{-k}$ structure of ABJM theory. Finally, the $2N\times 2N$ matrix $\mathbb{B}$ is the Jacobian relating the $\{x_i,\tilde{x}_j\}$ variables to the $\{e^{iB_i},e^{i\tilde{B}_j}\}$ variables

$$\mathbb{B} = \begin{pmatrix} x_l\frac{\partial e^{iB_j}}{\partial x_l} & \tilde{x}_l\frac{\partial e^{iB_j}}{\partial\tilde{x}_l} \\ x_l\frac{\partial e^{i\tilde{B}_j}}{\partial x_l} & \tilde{x}_l\frac{\partial e^{i\tilde{B}_j}}{\partial\tilde{x}_l}\end{pmatrix}. \tag{2.9}$$

It is convenient to introduce the chemical potentials Δ_a according to $y_a = e^{i\Delta_a}$. As discussed in [11], the general form of the eigenvalues for $k=1$ scales with $\sqrt{N}$ and is given by

$$u_i = iN^{1/2}t_i + v_i, \qquad \tilde{u}_i = iN^{1/2}t_i + \tilde{v}_i. \tag{2.10}$$

A remarkable result of [11] is the explicit treatment of Eq. (2.8) to yield, as the leading term for $k=1$ in an expansion in N

$$\mathrm{Re}\log Z = -\frac{N^{3/2}}{3}\sqrt{2\Delta_1\Delta_2\Delta_3\Delta_4}\sum_a\frac{n_a}{\Delta_a}. \tag{2.11}$$

A more comprehensive numerical analysis of the index and the subsequent subleading corrections in N was presented in [19]. The logarithmic in N contribution to the topologically twisted index was matched with the appropriate eleven-dimensional supergravity one-loop quantum computation in [21].

III. THE TOPOLOGICALLY TWISTED INDEX IN THE 'T HOOFT LIMIT

One of the main goals of this manuscript is to compute $\mathrm{Re}\log Z$ in the 't Hooft limit, that is, for $N\to\infty$ while $\lambda = N/k$ is held fixed. What follows below is essentially an analysis similar to the one performed in [11] for the M-theory limit but with a few observations meant to setup large N corrections to the "saddle point" computation.

Given our interest in extending the previous results of [11] to the 't Hooft limit, we are going to carefully and explicitly track the Chern-Simons level k in our manipulations. Under the change of variables $x_i = e^{iu_i}, \tilde{x}_j = e^{i\tilde{u}_j}, y_a = e^{i\Delta_a}$ one finds that the Bethe Ansatz equations become

$$0 = ku_i + i\sum_{j=1}^{N}\left[\sum_{a=3,4}\mathrm{Li}_1(e^{i(\tilde{u}_j-u_i+\Delta_a)}) - \sum_{a=1,2}\mathrm{Li}_1(e^{i(\tilde{u}_j-u_i-\Delta_a)})\right] - 2\pi n_i,$$
$$0 = k\tilde{u}_j + i\sum_{j=1}^{N}\left[\sum_{a=3,4}\mathrm{Li}_1(e^{i(\tilde{u}_j-u_i+\Delta_a)}) - \sum_{a=1,2}\mathrm{Li}_1(e^{i(\tilde{u}_j-u_i-\Delta_a)})\right] - 2\pi\tilde{n}_j, \tag{3.1}$$

where n_i and $\tilde{n}_j$ are integer numbers characterizing the ambiguity in solving $e^{iB_i} = e^{i\tilde{B}_j} = 1$ and the above system of equations. It is worth pointing out that the BAE are, in principle, exact equations determining the poles. Namely, they are not obtained in a large N limit and are valid to generate the topologically twisted index for any value of N and any value of k. We are ultimately, of course, interested in the regime where a comparison with supergravity can be made but the exactness of this approach should have powerful implications for an eventual string theoretic understanding of the topologically twisted index as providing ultraviolet complete quantum gravity data.

It is worth noting, as remarked in [11], that the above system of equations follows from the critical points of a "Bethe potential"

$$\mathcal{V} = \sum_{i=1}^{N}\left[\frac{k}{2}(\tilde{u}_i^2 - u_i^2) - 2\pi(\tilde{n}_i\tilde{u}_i - n_i u_i)\right] + \sum_{i,j=1}^{N}\left[\sum_{a=3,4}\mathrm{Li}_2(e^{i(\tilde{u}_j - u_i + \Delta_a)}) - \sum_{a=1,2}\mathrm{Li}_2(e^{i(\tilde{u}_j - u_i - \Delta_a)})\right]. \tag{3.2}$$

A. Numerical results: Eigenvalues and eigenvalue densities

A natural way to encode the behavior of the eigenvalues is through its density for which we use the density of the imaginary part $\rho(t)$ and that of the real part $\delta v(t)$. This transition from discrete to continuous distribution is standard in problems involving large N limits. Our computation will end up being a hybrid of sorts in the sense that we use large N technology with is ubiquitous introduction of eigenvalue densities but also rely on the exact numerical evaluation for finite N and the corresponding numerical fitting.

We start the analysis of the eigenvalues with the observation that a simple rescaling corresponding to the case discussed in [11] provides some intuition for the potential generalization to the 't Hooft limit: $t \mapsto t/\sqrt{k}, \rho \mapsto \rho\sqrt{k}$, $\delta v \mapsto \delta v$. It is then easy to confirm numerically that the behavior for small but arbitrary k takes the form:

$$u_i = iN^{1/2}\frac{t_i}{\sqrt{k}} + \frac{\pi}{k} - \frac{1}{2}\delta v(t_i),$$
$$\tilde{u}_i = iN^{1/2}\frac{t_i}{\sqrt{k}} + \frac{\pi}{k} + \frac{1}{2}\delta v(t_i). \tag{3.3}$$

The above expression already suggests a solution in the 't Hooft limit:

$$u_i = i\sqrt{\lambda}t_i + \pi\frac{\lambda}{N} - \frac{1}{2}\delta v(t_i),$$
$$\tilde{u}_i = i\sqrt{\lambda}t_i + \pi\frac{\lambda}{N} + \frac{1}{2}\delta v(t_i). \tag{3.4}$$

The basic principle for numerically solving large-scale equations like the BAE (3.1) is that the closer our starting point for the variables is to the final exact solution, the more probable and the faster it is to arrive at this solution through multidimensional root finding. Naturally, the strategy of solving the BAE is to start from the solution in the M-theory limit, that is, for small values of k and build up toward the solution in the IIA limit using the universal method of iteration. This method is based on the hypothesis that the eigenvalues change smoothly with the parameters in the equations which numerically translates into the fact that we should change the parameters of the BAE such as N and k (or λ) with a small step length. Details of the numerical algorithm are in Appendix A.

1. Special case: $\Delta_a = \pi/2$

An example of the numerical solution for the special case (all fugacities equal) is shown in Fig. 1 and the corresponding eigenvalue density $\rho(t)$ and function $\delta v(t)$ are shown in Fig. 2. The analytic leading order expressions for ρ and δv are the same as those in [11]

$$\rho(t) = \frac{1}{\sqrt{2}\pi}, \qquad \delta v(t) = \frac{t}{\sqrt{2}}, \quad \text{for } t \in \left[-\frac{\pi}{\sqrt{2}}, \frac{\pi}{\sqrt{2}}\right]. \tag{3.5}$$

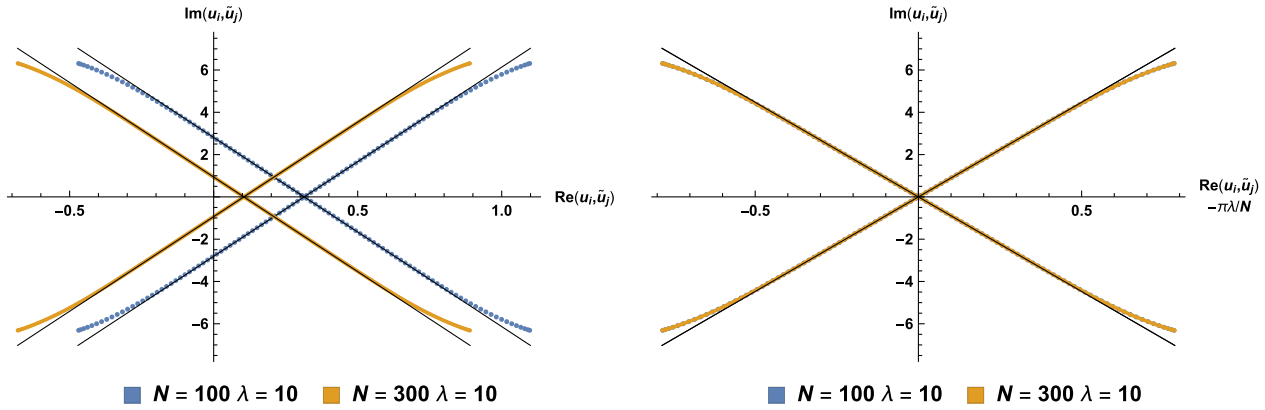

(a) Eigenvalue distribution (b) Eigenvalue distribution (translated to the origin)

FIG. 1. Eigenvalue distribution for the special case for two different values of N corresponding to $N = 100$ (blue) and 300 (orange) while keeping the same $\lambda = 10$.

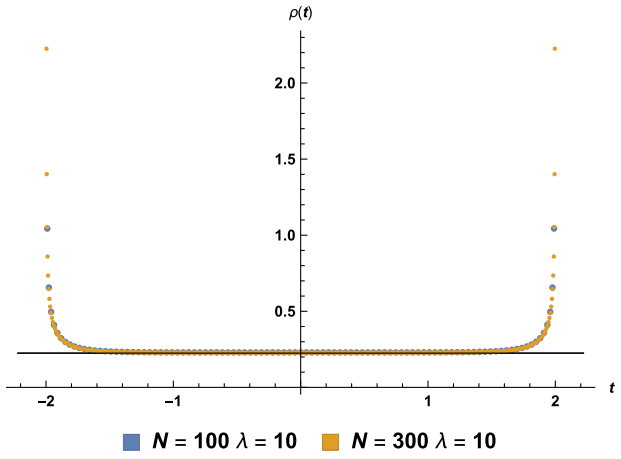

(a) Eigenvalue density $\rho(t)$

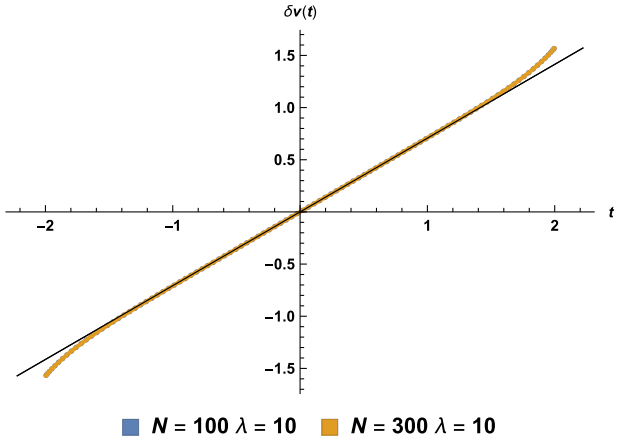

(b) Function $\delta v(t)$

FIG. 2. The eigenvalue density $\rho(t)$ and the function $\delta v(t)$ for the special case for $N = 100$ (blue) and 300 (orange) both for $\lambda = 10$.

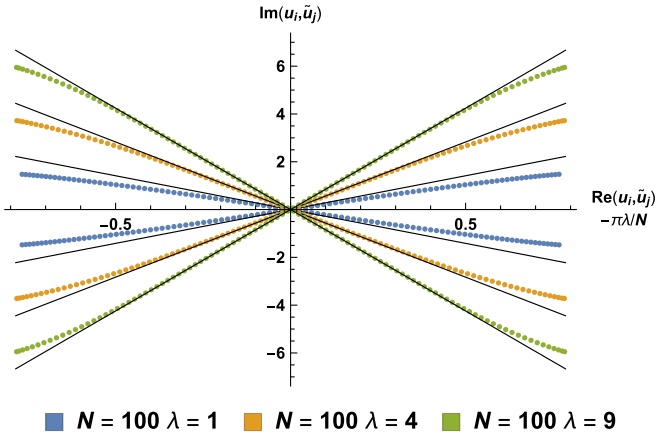

FIG. 3. Eigenvalue distribution (translated to the origin) for the special case for three different values of λ corresponding to $\lambda = 1$ (blue), 4 (orange) and 9 (green) while keeping the same $N = 100$.

These expressions correspond to the black lines in Fig. 2. The black lines in Figure 1 correspond to the analytical expressions in Eq. (3.4).

The overlapping position of the eigenvalues as shown in Fig. 1(b) as well as their continuous distributions Fig. 2(a) and 2(b) for quite different values of $N = 100$, 300 but corresponding to the same λ demonstrates numerically that the eigenvalue densities, in this limit are independent of N but depend only on λ.

The attentive reader might have noticed that the analytic expressions, plotted as continuous black lines in the plot differ somehow from the numerical values at the endpoints of the intervals. We will discuss these deviations in the context of generic fugacities where they are more prominent.

Having understood that the eigenvalue distribution depends only on λ we proceed to demonstrate numerically

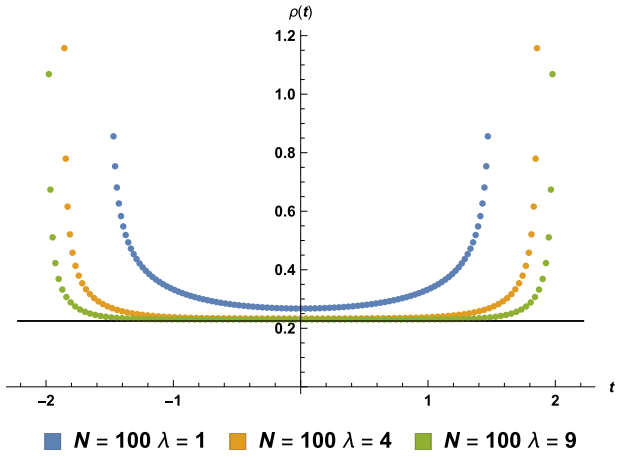

(a) Eigenvalue density $\rho(t)$

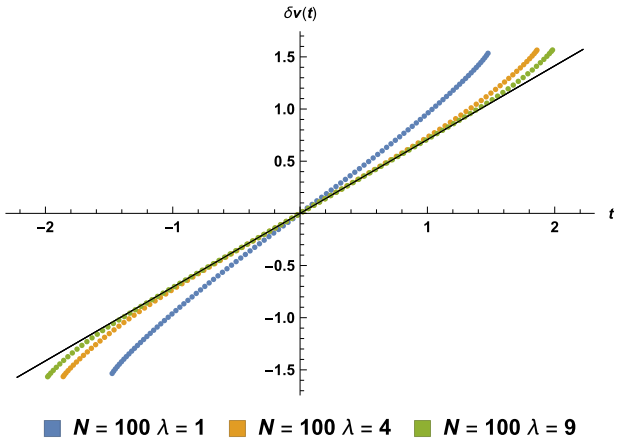

(b) Function $\delta v(t)$

FIG. 4. The eigenvalue density $\rho(t)$ and the function $\delta v(t)$ for the special case for $\lambda = 1$ (blue), 4 (orange) and 9 (green) all for $N = 100$.

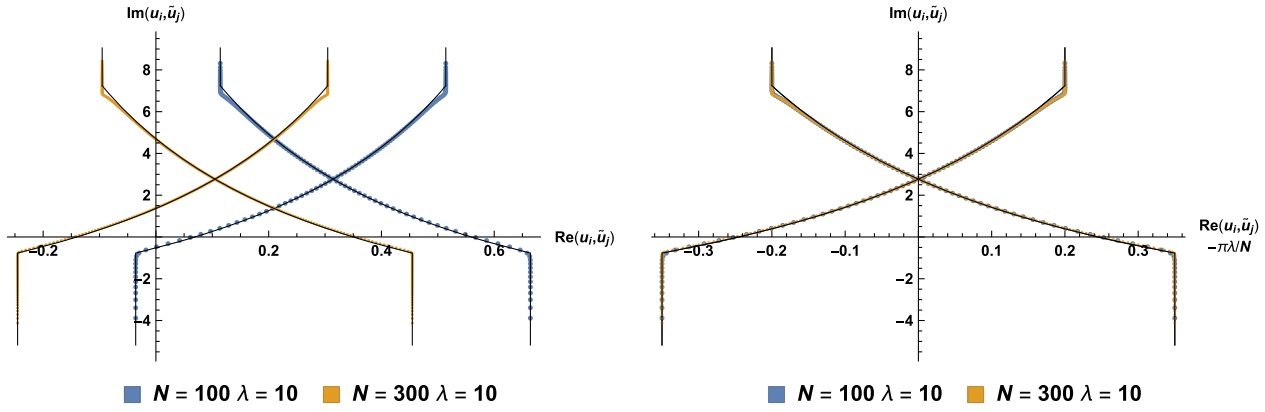

(a) Eigenvalue distribution

(b) Eigenvalue distribution (translated to the origin)

FIG. 5. Eigenvalue distribution for $\Delta_a = \{0.4, 0.5, 0.7, 2\pi - 1.6\}$ for two different values of N corresponding to $N = 100$ (blue) and 300 (orange) while keeping the same $\lambda = 10$.

that the scaling of the imaginary part is as $\sqrt{\lambda}$. In Figs. 3 and 4 we plot the eigenvalue distribution, the eigenvalue density $\rho(t)$ and the function $\delta v(t)$ for various values of $\lambda = 1, 4, 9$ for a given $N = 100$. It can be seen that the scaling is consistent with a behavior $\sqrt{\lambda}$. Note that the numerical results approach the black lines (analytical results) in Figs. 3 and 4 as one increases the value of λ. We thus expect that the agreement with gravity becomes better precisely in this regime of large λ. We will explicitly elucidate this effect when fitting the full topologically twisted index.

Note that the solution with all equal fugacities has ρ constant which points to similarities with computations in the matrix model limit of ABJM free energy on S^3 [26]. Such similarities between the behavior of the free energy and the topologically twisted index were noted in the M-theory limit previously in, for example, [27,28]. We now see that there is a natural generalization of such relations in the 't Hooft limit as well.

2. General case: generic Δ_a

The special case is particularly well behaved numerically. Below we present analogous results for the case of generic values of the fugacities Δ_a. The conclusions are the same as those drown in the special case. The numerical solution for $\Delta_a = \{0.4, 0.5, 0.7, 2\pi - 1.6\}$ is shown in Fig. 5 and the corresponding eigenvalue density $\rho(t)$ and function $\delta v(t)$ are shown in Fig. 6. The overlapping plots demonstrate numerically that the structure of the eigenvalues coincides for a given value of λ and are independent of N in the large N limit.

The scaling of the imaginary part with $\sqrt{\lambda}$ and the trend that larger values of λ lead to a better matching between the

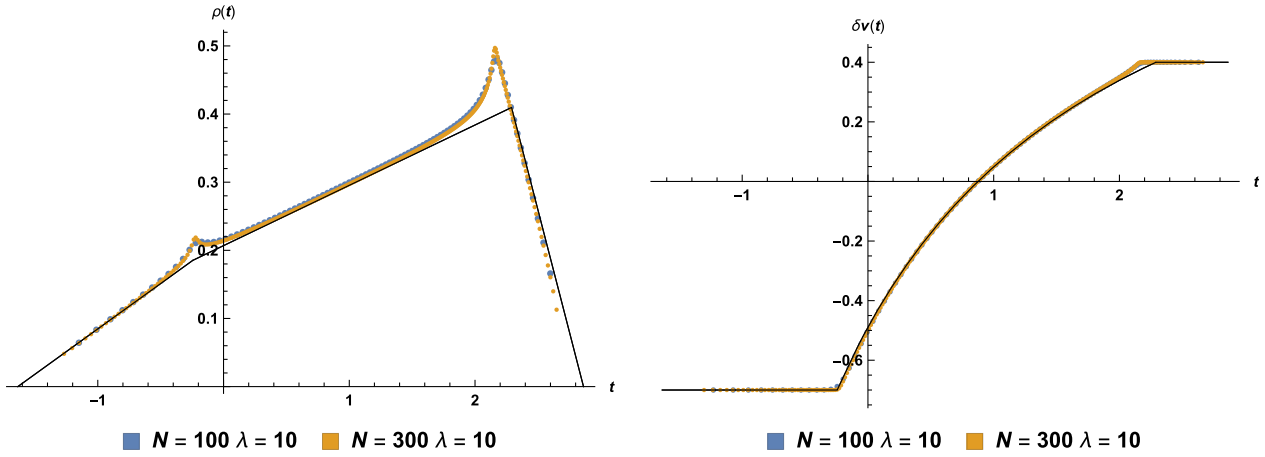

(a) Eigenvalue density $\rho(t)$

(b) Function $\delta v(t)$

FIG. 6. The eigenvalue density $\rho(t)$ and the function $\delta v(t)$ for $\Delta_a = \{0.4, 0.5, 0.7, 2\pi - 1.6\}$ for $N = 100$ (blue) and 300 (orange) both for $\lambda = 10$.

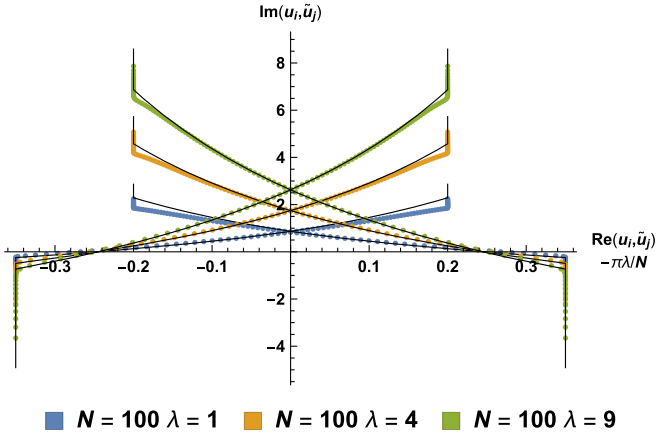

FIG. 7. Eigenvalue distribution (translated to the origin) for $\Delta_a = \{0.4, 0.5, 0.7, 2\pi - 1.6\}$ for three different values of λ corresponding to $\lambda = 1$ (blue), 4 (orange) and 9 (green) while keeping the same $N = 100$.

numerical result and the analytic leading expression are also on display in Figs. 7 and 8. The effect on the tails seems to be clearly dominated by λ and, again, becomes smaller the larger the value of λ. Figures 7 and 8 are all plotted for $N = 100$ and we appreciate, even with the naked eye, the reduction of the effect of the tails as λ increases.

B. The index

In this section we perform a fitting of our results. The leading part of the index can be computed analytically based on the structure of the eigenvalue densities. Having established the behavior Eq. (3.4) of the eigenvalue distribution in the large N, large λ limit we can proceed to analytically evaluate the topologically twisted index in the 't Hooft limit. Our starting point is the Bethe potential Eq. (3.2). We evaluate various parts of $\mathcal{V}$ largely following the techniques employed in [11]. Consider the first term in Eq. (3.2) in the large N limit it becomes

$$\frac{N}{2\lambda}\sum_{i=1}^{N}(\tilde{u}_i^2 - u_i^2) = \frac{N}{2\lambda}\sum_{i=1}^{N}\delta v_i\left(2i\sqrt{\lambda}t_i + \frac{2\pi\lambda}{N}\right) = \frac{iN^2}{\sqrt{\lambda}}\int dt\rho(t)t\delta v(t) + \mathcal{O}(N). \tag{3.6}$$

Considering another term one can show that in the large N limit

$$\sum_{i<j}\mathrm{Li}_2(e^{i(\tilde{u}_j - u_i - \Delta)}) \mapsto N^2\int dt\rho(t)\int_t dt'\rho(t')\mathrm{Li}_2(e^{i(\tilde{u}(t') - u(t) + \Delta)}). \tag{3.7}$$

Following [11] (see also [26]) we study the behavior of this term using its expansion, namely, recall that

$$\mathrm{Li}_n(e^{iu}) = \sum_{m=1}^{\infty}\frac{e^{imu}}{m^n}. \tag{3.8}$$

We approximate part of the integral appearing in Eq. (3.7) using a Taylor expansion and then noticing that each subsequent term is ultimately suppressed by $1/\sqrt{\lambda}$. Namely,

$$I_m(t) = \int_t dt'\rho(t')e^{im(\tilde{u}(t') - u(t) + \Delta)} = \int_t e^{-m\sqrt{\lambda}(t'-t)}\sum_{j=0}^{\infty}\frac{(t'-t)^j}{j!} \times \partial_x^j[\rho(x)e^{im(\frac{\delta v(x)}{2} + \frac{\delta v(t)}{2} + \Delta)}]|_{x=t} \tag{3.9}$$

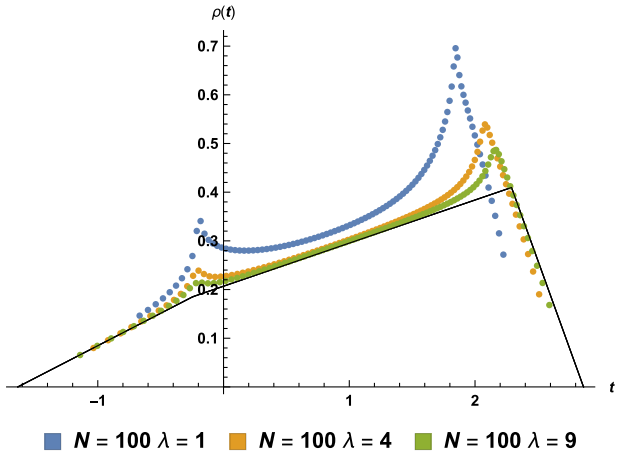

(a) Eigenvalue density $\rho(t)$

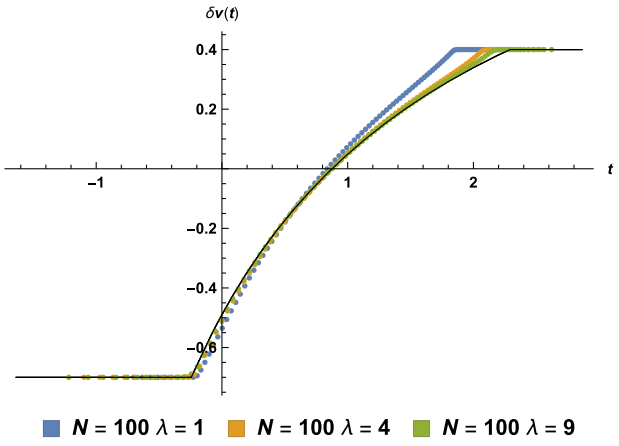

(b) Function $\delta v(t)$

FIG. 8. The eigenvalue density $\rho(t)$ and the function $\delta v(t)$ for $\Delta_a = \{0.4, 0.5, 0.7, 2\pi - 1.6\}$ for $\lambda = 1$ (blue), 4 (orange) and 9 (green) all for $N = 100$.

$$= \frac{1}{\sqrt{\lambda}} \frac{\rho(t)}{m} e^{im(\delta v(t)+\Delta)} + \mathcal{O}(\lambda^{-1}), \tag{3.10}$$

where in the second line we have introduced a Taylor expansion around $t' = t$ and in the last line we have taken the large λ limit.

Therefore we conclude that in the large N and further large λ limit, the leading contribution is of the form:

$$\sum_{i<j} \mathrm{Li}_2(e^{i(\tilde{u}_j - u_i + \Delta)}) \mapsto \frac{N^2}{\sqrt{\lambda}} \int dt \rho^2(t) \mathrm{Li}_3(e^{i(\delta v(t)+\Delta)}). \tag{3.11}$$

Similar types of manipulations in the Bethe potential lead to one of the main results of this section, the fact that our Bethe potential can be written as

$$\begin{aligned} \mathcal{V} = \frac{iN^2}{\sqrt{\lambda}} \int dt \Bigg[& t\rho(t)\delta v(t) \\ & + \rho^2(t) \Bigg(\sum_{a=3,4} g_+(\delta v(t) + \Delta_a) - \sum_{a=1,2} g_-(\delta v(t) - \Delta_a) \Bigg) \Bigg] \\ & - \mu \Bigg[\int dt \rho(t) - 1 \Bigg], \end{aligned} \tag{3.12}$$

where

$$g_\pm(u) = \frac{1}{6}u^3 \mp \frac{\pi}{2}u^2 + \frac{\pi^2}{3}u, \tag{3.13}$$

and μ is a Lagrange multiplier enforcing the normalization of the eigenvalue density. This is precisely the same Bethe potential discussed in [11] except for the overall factor, here $N^2/\sqrt{\lambda}$ while there $N^{3/2}$. Some preliminary analysis in [19] showed that, as expected, for small values of k, the scaling is indeed $N^{3/2}k^{1/2}$. The main conclusion following Eq. (3.12) and its similarity with the Bethe potential in the M-theory limit of the potential in [11] is that, therefore, all the extremization procedure is precisely as in [11]. One can also refer to the more general analysis connecting Bethe potentials to topologically twisted indices [27] to conclude that to leading order one has

$$\boxed{\mathrm{Re}\log Z_0 = -\frac{1}{3}\frac{N^2}{\sqrt{\lambda}} \sqrt{2\Delta_1\Delta_2\Delta_3\Delta_4} \sum_a \frac{n_a}{\Delta_a}.} \tag{3.14}$$

What we need to keep in mind is that in the 't Hooft limit, our result also uses the large λ limit. Indeed, there are potential corrections to the leading term of the order $\mathcal{O}(N^2/\lambda)$. This is best seen in Eq. (3.10) and clarifies the deviation between the numerical and analytic results for small values of lambda that was glanced already in the analysis of eigenvalues depicted in Figs. 7 and 8. The deviation was largest for the smallest value of λ and decreased as λ was increased.

1. Potential corrections to the leading order: $N^2/\sqrt{\lambda}$ vs N^2/λ

To better understand the potential corrections to the leading order term let us revisit the above computation of the Bethe potential. One crucial step in taking the large N limit is the evaluation in Eq. (3.11). Let us repeat the derivation with more details here:

$$\begin{aligned} \sum_{i<j} \mathrm{Li}_2(e^{i(\tilde{u}_j - u_i + \Delta)}) &\mapsto N^2 \int dt \rho(t) \int_t dt' \rho(t') \mathrm{Li}_2(e^{i(\tilde{u}(t') - u(t) + \Delta)}) \\ &= N^2 \int dt \rho(t) \sum_{m=1}^{\infty} \frac{I_m(t)}{m^2}, \end{aligned} \tag{3.15}$$

where

$$\begin{aligned} I_m(t) &= \int_t dt' e^{-m\sqrt{\lambda}(t'-t)} \sum_{j=0}^{\infty} \frac{(t'-t)^j}{j!} \partial_x^j [\rho(x) e^{im(\frac{\delta v(x)}{2} + \frac{\delta v(t)}{2} + \Delta)}]|_{x=t} = \sum_{j=0}^{\infty} I_m^{(j)}(t), \\ I_m^{(j=0)} &= \frac{1}{m\sqrt{\lambda}} \rho(t) e^{im(\delta v(t)+\Delta)}, \\ I_m^{(j=1)} &= \frac{1}{(m\sqrt{\lambda})^2} \partial_x [\rho(x) e^{im(\frac{\delta v(x)}{2} + \frac{\delta v(t)}{2} + \Delta)}]|_{x=t} \\ &= \frac{1}{m^2\lambda} \rho'(t) e^{im(\delta v(t)+\Delta)} + \frac{i}{2m\lambda} \rho(t) \delta v'(t) e^{im(\delta v(t)+\Delta)}, \\ I_m^{(j\geq 2)} &= \frac{1}{(m\sqrt{\lambda})^{j+1}} \partial_x^j [\rho(x) e^{im(\frac{\delta v(x)}{2} + \frac{\delta v(t)}{2} + \Delta)}]|_{x=t}. \end{aligned} \tag{3.16}$$

Therefore:

$$\sum_{i<j}\mathrm{Li}_2(e^{i(\tilde{u}_j-u_i+\Delta)}) \mapsto N^2\int dt\rho(t)\sum_{m=1}^{\infty}\frac{1}{m^2}\sum_{j=0}^{\infty}I_m^{(j)}(t)$$
$$=\frac{N^2}{\sqrt{\lambda}}\int dt\rho(t)^2\mathrm{Li}_3(e^{i(\delta v(t)+\Delta)})+\frac{N^2}{\lambda}\int dt\rho(t)\left[\rho'(t)\mathrm{Li}_4(e^{i(\delta v(t)+\Delta)})+\frac{i}{2}\rho(t)\delta v'(t)\mathrm{Li}_3(e^{i(\delta v(t)+\Delta)})\right]$$
$$+\sum_{j=2}^{\infty}\frac{N^2}{\lambda^{(j+1)/2}}\int dt\rho(t)\sum_{m=1}^{\infty}\frac{1}{m^{j+3}}\partial_x^j[\rho(x)e^{im(\frac{\delta v(x)}{2}+\frac{\delta v(t)}{2}+\Delta)}]|_{x=t}. \tag{3.17}$$

Given that the distributions $\rho(t)$ and $\delta v(t)$ are piecewise linear functions at the leading order, we learn from the above expansion that the subleading contributions are more pronounced in the neighborhoods where the functions change their slopes. A similar behavior was noted in the M-theory limit treatment [11,19] and dubbed contributions from the tails; here, as indicated numerically in Figs. 7 and 8, the controlling parameter is $1/\sqrt{\lambda}$ and makes it harder to numerically suppress the contribution from the tails.

2. Free energy in the 't Hooft limit of ABJM

A good model for the subleading structure of the index can be inferred from the behavior of the free energy on S^3. The 't Hooft limit of the free energy on S^3 for the ABJM theory has been worked out in a series of publications, see, for example [2,3,29]. The main result of those publications is that the $1/N$ expansion of the free energy takes the form

$$F(\lambda,g_s)=\sum_{g=0}^{\infty}g_s^{2g-2}F_g(\lambda), \tag{3.18}$$

where

$$g_s=\frac{2\pi i}{k},\qquad \lambda=\frac{N}{k}. \tag{3.19}$$

To be completely precise k is not to appear at all in the above expression and the appropriate way to read it is

$$F(\lambda,N)=\sum_{g=0}^{\infty}\left(\frac{2\pi i\lambda}{N}\right)^{2g-2}F_g(\lambda). \tag{3.20}$$

The explicit dependence on λ in $F_g(\lambda)$ is best stated through a variable κ such that

$$\lambda(\kappa)=\frac{\kappa}{8\pi}{}_3F_2\left(\frac{1}{2},\frac{1}{2},\frac{1}{2};1,\frac{3}{2};-\frac{\kappa^2}{16}\right), \tag{3.21}$$

where ${}_3F_2$ is the generalized hypergeometric function.

The quantity we are interested at the subleading order, $F_1(\lambda)$, is naturally written in terms of another variable τ which is related to κ as follows:

$$\tau=i\frac{K'(\frac{i\kappa}{4})}{K(\frac{i\kappa}{4})}, \tag{3.22}$$

where K is the complete elliptic integral of the first kind. In this new variable τ we have

$$F_1(\lambda(\tau))=-\log\eta(\tau), \tag{3.23}$$

where $\eta(\tau)$ is the Dedekind eta function.

The expansion for the free energy $F(\lambda,N)$ is to be understood as taking very large N first, and then considering its dependence on λ. In the strong coupling regime $\lambda\to\infty$ or $\kappa\to\infty$, it is convenient to use the shifted variable for relationship between λ and κ:

$$\hat{\lambda}=\lambda-\frac{1}{24}=\frac{1}{2\pi^2}\log^2\kappa+\mathcal{O}(\kappa^{-2}),\quad \kappa\gg 1. \tag{3.24}$$

For very large N the two leading terms are $F_0(\lambda)$ and $F_1(\lambda)$ corresponding in the topological expansion Eq. (3.20) to genus $g=0$ and genus $g=1$, respectively. At strong coupling we get:

$$F_0(\lambda)=\frac{4\pi^3\sqrt{2}}{3}\hat{\lambda}^{3/2}+\mathcal{O}(e^{-2\pi\sqrt{2\hat{\lambda}}}),$$
$$F_1(\lambda)=\frac{1}{6}\log\kappa-\frac{1}{2}\log\left[\frac{2\log\kappa}{\pi}\right]+\mathcal{O}(\kappa^{-2})$$
$$=\frac{\pi}{6}\sqrt{2\hat{\lambda}}-\frac{1}{4}\log\hat{\lambda}-\frac{3}{4}\log 2+\mathcal{O}(e^{-2\pi\sqrt{2\hat{\lambda}}}). \tag{3.25}$$

For $g\geq 0$, the leading, strong coupling behavior is given by [3]:

$$F_g(\lambda)\sim\lambda^{\frac{3}{2}-g},\qquad \lambda\to\infty, g\geq 0. \tag{3.26}$$

Note that to obtain the contribution to the actual free energy we need to recall that this term comes multiplied by g_s^{-2}. If we neglect the small shift $-1/24$ for large λ, the leading term is

$$F_{\text{Leading}} = g_s^{-2} F_0(\lambda) = g_s^{-2} \frac{4\pi^3\sqrt{2}}{3}\lambda^{3/2} = \left(\frac{2\pi i\lambda}{N}\right)^{-2} \frac{4\pi^3\sqrt{2}}{3}\lambda^{3/2} = -\frac{\pi\sqrt{2}}{3}\frac{N^2}{\sqrt{\lambda}}. \tag{3.27}$$

This is the quantity that was shown to perfectly match the on-shell action for supergravity on $AdS_4 \times \mathbb{CP}^3$ [2]. We have already shown here that the scaling agrees with the leading behavior Eq. (3.14) of the topologically twisted index in the 't Hooft limit.

To develop some intuition into the sub-leading behavior we might expect for the index we turn to the analogous quantity for the free energy, $F_1(\lambda)$. Note that F_1 contributes to the free energy with no powers of g_s as corresponds to the genus one term. Therefore the leading and subleading contribution to the free energy are:

$$F_{\text{Leading and Subleading}} = -\frac{\pi\sqrt{2}}{3}\frac{N^2}{\sqrt{\lambda}} + N^0\left[\frac{\pi}{6}\sqrt{2\lambda} - \frac{1}{4}\log\lambda - \frac{3}{4}\log 2\right] + \sum_{g=2}^{\infty}\left(\frac{2\pi i\lambda}{N}\right)^{2g-2} F_g(\lambda), \tag{3.28}$$

where

$$\sum_{g=2}^{\infty}\left(\frac{2\pi i\lambda}{N}\right)^{2g-2} F_g(\lambda) \sim \sum_{g=2}^{\infty} N^{2-2g}\lambda^{g-1/2}. \tag{3.29}$$

This approximation is the crucial one and we will show how it informs our fitting results. We will fit our numerical results following the structure of the free energy. The genus expansion predicts terms of the form N^{2-2g}, $g = 0, 1, 2, \ldots$. The behavior of the F_1 term in the appropriate limit it leads to a logarithmic dependence of the type

$$-\frac{1}{4}\log\lambda. \tag{3.30}$$

We, therefore, expect an analogous term for the topologically twisted index.

3. Numerical results: The leading term of the index

Having obtained the leading order expression analytically and the guidance from the free energy on S^3, we now proceed to consider subleading contributions to the topologically twisted index of ABJM. We expand the index beyond the leading order in N and we expect the subleading behavior of the index to have the form

$$\text{Re}\log Z = f_1(\lambda, \Delta_a, n_a)N^2 + f_2(\lambda, \Delta_a, n_a)\log N + f_3(\lambda, \Delta_a, n_a) + \mathcal{O}(N^{-2}), \tag{3.31}$$

where the functions f_1, f_2 and f_3 are linear in the magnetic fluxes n_a. Our goal is to numerically clarify the structure of the functions f_1, f_2 and f_3. The function f_1 clearly defines the leading term, the function f_2 deserves some explanation in the current context which we now provide. It is well known [30] that there are terms that can be present in the exact expression for certain partition functions but are not captured in the 't Hooft limit. This is typical in the context of Chern-Simons theories as explained in detail in [30]; the precise reason being the residual global gauge symmetries corresponding to constant $U(N)$ gauge transformations. As a result, the nonperturbative partition function contains a volume factor which ultimately is responsible for $\log N$ terms in the exact evaluation which are not captured by the 't Hooft expansion. Our numerical computation, being exact, does indeed contain such $\log N$ term and we take it into consideration when fitting by introducing the f_2 function.[1]

For a given set of chemical potentials Δ_a and a fixed λ, we compute the index Eq. (2.8) and its real part $\text{Re}\log Z$ for a range of N. Since the solutions are "k-fold degenerate" for $k > 1$, we should sum over all the orbits and multiply the index by $k = (N/\lambda)$ [11]. We then decompose $\text{Re}\log Z$ into a sum of four independent terms

$$\text{Re}\log Z = A + B_1 n_1 + B_2 n_2 + B_3 n_3, \tag{3.32}$$

where we have used the condition $\sum_a n_a = 2$. Then we perform a linear least-squares fit for A and B_a to the function

$$f(N) = f_1 N^2 + f_2\log N + f_3 + \sum_{g=2}^{g_c} f_{g+2} N^{2-2g}, \tag{3.33}$$

where g_c is the cutoff value of the genus g. Since the largest value of N is finite (about 300), it is important to consider the inverse powers of N. Guided by numerical stability which has been checked in various regimes, the more subleading terms added in the fitting, the more accurate the fitting results will be. The maximum number of the fitting terms equals the number of N, but the real number of the fitting terms is always less than the maximum to avoid the over-fitting problem.

The results of the numerical fit for $\text{Re}\log Z$ with N are presented in Table I. The numerical results indicate that the coefficient f_2 of the $\log N$ term is precisely $2/3$.

The comparison between the numerical leading term $f_1 N^2$ and the analytical leading term $\text{Re}\log Z_0$ for the

[1]We thank Kazumi Okuyama for important clarifications on this point.

TABLE I. Numerical fit for $\mathrm{Re}\log Z = f_1 N^2 + f_2 \log N + f_3 + \cdots$. The values of N used in the fit range from 100 to 300 in steps of 10 for the special case and from 50 to 300 in steps of 10 for the general cases. We made use of the fact that the index is independent of the magnetic fluxes when performing the fit for the special case ($\Delta_a = \{\pi/2, \pi/2, \pi/2, \pi/2\}$).

λ	Δ_1	Δ_2	Δ_3	f_1	f_2	f_3
1	$\pi/2$	$\pi/2$	$\pi/2$	-1.43536	0.66667	0.82149
	0.3	0.4	0.5	-0.13041	0.66667	4.45202
				$-0.75745n_1$	$+2.11753\times10^{-17}n_1$	$-0.11447n_1$
				$-0.55716n_2$	$-8.54078\times10^{-20}n_2$	$-0.44612n_2$
				$-0.44271n_3$	$-8.55415\times10^{-20}n_3$	$-0.35008n_3$
	0.4	0.5	0.7	-0.19246	0.66667	3.43678
				$-0.80669n_1$	$+2.30654\times10^{-20}n_1$	$-0.08378n_1$
				$-0.63097n_2$	$+3.85179\times10^{-23}n_2$	$-0.31636n_2$
				$-0.43713n_3$	$-2.71336\times10^{-23}n_3$	$-0.25899n_3$
5	$\pi/2$	$\pi/2$	$\pi/2$	-0.65587	0.66667	2.62506
	0.3	0.4	0.5	-0.04701	0.66667	12.48909
				$-0.36002n_1$	$+1.59689\times10^{-6}n_1$	$-0.52544n_1$
				$-0.26436n_2$	$+3.19791\times10^{-8}n_2$	$-1.23230n_2$
				$-0.20773n_3$	$-1.80238\times10^{-8}n_3$	$-1.18290n_3$
	0.4	0.5	0.7	-0.07381	0.66667	9.85037
				$-0.38478n_1$	$+5.93294\times10^{-8}n_1$	$-0.41298n_1$
				$-0.30060n_2$	$+2.56635\times10^{-9}n_2$	$-0.90099n_2$
				$-0.20521n_3$	$-3.06747\times10^{-10}n_3$	$-0.90971n_3$
10	$\pi/2$	$\pi/2$	$\pi/2$	-0.46585	0.66667	4.56578
	0.3	0.4	0.5	-0.03264	0.66699	19.08969
				$-0.25646n_1$	$+0.00037n_1$	$-0.82192n_1$
				$-0.18831n_2$	$+0.00003n_2$	$-1.81001n_2$
				$-0.14765n_3$	$-5.06570\times10^{-6}n_3$	$-1.80619n_3$
	0.4	0.5	0.7	-0.05168	0.66671	15.22590
				$-0.27410n_1$	$+0.00004n_1$	$-0.64388n_1$
				$-0.21415n_2$	$+4.99553\times10^{-6}n_2$	$-1.32871n_2$
				$-0.14585n_3$	$-5.58231\times10^{-7}n_3$	$-1.39319n_3$

special case is shown in Table II. Thus, showing that the numerical and the analytical values approach each other with increasing λ to a precision of the order of half a percent.

Now we focus on the relationship between f_1 and λ. From the corrections of the leading term in Eq. (3.17), we expect the behavior of the leading term f_1 to have the form

$$f_1(\lambda, \Delta_a, n_a) = g_1(\Delta_a, n_a)\frac{1}{\sqrt{\lambda}} + g_2(\Delta_a, n_a)\frac{1}{\lambda} + \mathcal{O}(\lambda^{-\frac{3}{2}}). \tag{3.34}$$

TABLE II. The comparison between the numerical and the analytical values of the leading term for the special case.

λ	f_1	$\mathrm{Re}\log Z_0/N^2$	Error
1	-1.43536	-1.48096	3.177%
5	-0.65587	-0.66231	0.982%
10	-0.46585	-0.46832	0.530%

Using a similar decomposition

$$f_1(\lambda, \Delta_a, n_a) = C + D_1 n_1 + D_2 n_2 + D_3 n_3, \tag{3.35}$$

we perform a linear least-squares fit of C and D_a to the function

$$g(\lambda) = g_1\frac{1}{\sqrt{\lambda}} + g_2\frac{1}{\lambda} + g_3\frac{1}{\lambda^{3/2}} + g_4\lambda^{-2} + \sum_{j=4}^{j_c} g_{j+1}\lambda^{-(j+1)/2}, \tag{3.36}$$

where j_c is the cutoff value of j, which is similar to g_c in Eq. (3.33). It is implied in Eq. (3.29) that the larger value of λ, the larger error of the fitting results, because we have to make a cutoff in the fitting and retain finite subleading terms in N. Thus λ should not be too large, especially for the general cases it is required that $\lambda \ll N$.

The results of the numerical fit for f_1 with λ are presented in Table III. One important numerical result is

TABLE III. Numerical fit for $f_1 = g_1/\sqrt{\lambda} + g_2/\lambda + g_3/\lambda^{3/2} + g_4\lambda^{-2} + \cdots$. In the fit, for the special case, λ ranges from 20 to 50 in steps of 5 and N ranges from 100 to 400 in steps of 10; for the general cases, λ ranges from 5 to 15 in steps of 1 and N ranges from 50 to 250 in steps of 5.

Δ_1	Δ_2	Δ_3	g_1	g_2	g_3	g_4
$\pi/2$	$\pi/2$	$\pi/2$	-1.48096	6.82484×10^{-8}	0.09256	0.04567
0.3	0.4	0.5	-0.10234	-0.00152	0.02172	-0.14090
			$-0.81680n_1$	$+0.00352n_1$	$+0.01924n_1$	$+0.19326n_1$
			$-0.59953n_2$	$-0.00230n_2$	$+0.06301n_2$	$-0.15096n_2$
			$-0.47071n_3$	$+0.01714n_3$	$-0.10581n_3$	$+0.65523n_3$
0.4	0.5	0.7	-0.16278	-0.00283	0.03041	-0.13613
			$-0.87298n_1$	$+0.00245n_1$	$+0.04017n_1$	$+0.06357n_1$
			$-0.68142n_2$	$-0.00644n_2$	$+0.09167n_2$	$-0.21940n_2$
			$-0.46418n_3$	$+0.00423n_3$	$+0.00489n_3$	$+0.05864n_3$

that, for the special case, the leading coefficient g_1 of the $N^2/\sqrt{\lambda}$ term matches the analytical value precisely in Eqs. (3.14) and (3.27)

$$g_1 = -1.48096 = -\frac{\pi\sqrt{2}}{3}. \tag{3.37}$$

For the cases of generic fugacities the leading coefficient also matches the analytical expression in Eq. (3.14).

It is worth pointing out that the numerical value in Table III of the coefficient g_2 of the N^2/λ term in Eq. (3.36) is vanishingly small. This is despite our original analytical estimation in Eq. (3.17). What the numerical approach is showing is that there is a sharp cancellation among the various terms contributing at N^2/λ order. Such cancellations are possible due to the symmetries of the ABJM model, at a more technical level they are consequences of identities among various polylogarithms. They have not been explored in the 't Hooft limit and we hope to return to an analytic proof in a separate publication. In fact, the absence of the N^2/λ term exactly corresponds to the absence of the $\mathcal{O}(N)$ term in the M-theory limit in [19], as we will argue later in this section.

Finally, the numerical analysis remarkably captures the shift $-1/24$ in λ in Eq. (3.24). Indeed, through Taylor expansion, the expression for the leading free energy of ABJM on S^3 becomes [3]:

$$\begin{aligned} F_{\text{Leading}} &= g_s^{-2}\frac{4\pi^3\sqrt{2}}{3}\hat{\lambda}^{3/2} \\ &= -\frac{\pi\sqrt{2}}{3}\frac{N^2}{\sqrt{\lambda}} + \frac{\pi}{24\sqrt{2}}\frac{N^2}{\lambda^{3/2}}. \end{aligned} \tag{3.38}$$

This shifted result agrees perfectly with the numerical analysis. Note that for the special case in Table III, the coefficient g_3 of the $N^2/\lambda^{3/2}$ term is precisely

$$g_3 = 0.09256 = \frac{\pi}{24\sqrt{2}}. \tag{3.39}$$

4. Numerical results: The first subleading term of the index

Next we explore the dependence of the first subleading term of the index, namely the function f_3 of the N^0 term, on λ. From the topological expansion of the free energy on S^3 to genus $g = 0$ and genus $g = 1$ in Eq. (3.28), we expect the behavior of the function f_3 to adhere to the following pattern

$$\begin{aligned} f_3(\lambda, \Delta_a, n_a) = {} & h_1(\Delta_a, n_a)\sqrt{\lambda} + h_2(\Delta_a, n_a)\log\lambda \\ & + h_3(\Delta_a, n_a) + \mathcal{O}(e^{-\sqrt{\lambda}}). \end{aligned} \tag{3.40}$$

Through the same decomposition we consider

$$f_3(\lambda, \Delta_a, n_a) = E + F_1 n_1 + F_2 n_2 + F_3 n_3, \tag{3.41}$$

and perform a linear least-squares fit of E and F_a to the function

$$h(\lambda) = h_1\sqrt{\lambda} + h_2\log\lambda + h_3. \tag{3.42}$$

The results of the numerical fit for f_3 with λ are presented in Table IV. The numerical results show that the coefficient h_2 of the $\log\lambda$ term is $-7/6$.

Similar to the comparison performed in [19], for the special case we find the approximate expression

$$h_1 = 2.96129 \approx \frac{2\pi}{3}\sqrt{2}. \tag{3.43}$$

A similar term, proportional to $\sqrt{\lambda}$, appears at genus one order in the topological expansion of the free energy on S^3 of the ABJM theory. It was argued that in the field theory

TABLE IV. Numerical fit for $f_3 = h_1\sqrt{\lambda} + h_2 \log\lambda + h_3$. In the fit, for the special case, λ ranges from 20 to 50 in steps of 5 and N ranges from 100 to 400 in steps of 10; for the general cases, λ ranges from 5 to 15 in steps of 1 and N ranges from 50 to 250 in steps of 5. To be more accurate, we replace λ with $\hat{\lambda} = \lambda - 1/24$ in the fit.

Δ_1	Δ_2	Δ_3	h_1	h_2	h_3
$\pi/2$	$\pi/2$	$\pi/2$	2.96129	−1.16397	−2.10347
0.3	0.4	0.5	7.96583	−1.14322	−3.41833
			$-0.30541n_1$	$-0.01480n_1$	$+0.17809n_1$
			$-0.61946n_2$	$-0.00297n_2$	$+0.15182n_2$
			$-0.66859n_3$	$-0.00320n_3$	$+0.31098n_3$
0.4	0.5	0.7	6.65321	−1.15405	−3.11676
			$-0.23751n_1$	$-0.01422n_1$	$+0.13854n_1$
			$-0.45679n_2$	$-0.00479n_2$	$+0.12381n_2$
			$-0.52009n_3$	$-0.00048n_3$	$+0.24913n_3$

dual it originates as instanton effects due to tunneling of eigenvalues in the respective matrix model. On the gravity side this very term was attributed to D2 brane instantons wrapping a warped $\mathbb{RP}^3$ inside $\mathbb{CP}^3$ [3] (see also [31] for a detailed treatment of instanton corrections). It is plausible that a similar origin is at play in our context of the topologically twisted index. On the gravity side, as we will see in the next section, the structure of $\mathbb{CP}^3$ is deformed due to the magnetic charges, which makes the D2 brane argument more subtle. Another promising venue to explore is along the lines of higher curvature corrections which, as shown in [32], might give rise to $\sqrt{\lambda}$ contributions for theories on AdS_4.

Thus, the topologically twisted index in the special case when all the fugacities take the same value, $\Delta_a = \pi/2$, is approximately of the form

$$\begin{aligned}\mathrm{Re}\log Z(\Delta_a = \pi/2) = &-\frac{\pi\sqrt{2}}{3}\frac{N^2}{\sqrt{\lambda}} + \frac{2}{3}\log N + \frac{2\pi}{3}\sqrt{2\lambda} \\ &-\frac{7}{6}\log\lambda + \mathcal{O}(1) + \mathcal{O}(N^{-2}).\end{aligned} \tag{3.44}$$

One of our main results in this manuscript is the prediction, from the field theory side, for the term $-(7/6)\log\lambda$; this seems to be persistent and robust for generic values of the fugacities as indicated numerically in Table IV. This term, as christened by Ashoke Sen in a series of papers [33,34], constitutes an infrared window into ultraviolet physics. Here we have obtained it by exploring the field theory side which via the AdS/CFT correspondence provides an ultraviolet complete description of the dual gravity. The very same term should be reproduced by a one-loop computation on the gravity side using only the massless sector. In the context of asymptotically flat black holes in string theory such logarithmic corrections have been reproduced in a variety of situations [35]. In asymptotically AdS spacetimes positive results have been reported in the M-theory limit [21,25,36]; it would be quite interesting to reproduce such logarithmic correction in the 't Hooft limit from the dual type IIA supergravity.

Let us conclude this section with an extra sanity check. In the M-theory limit it was found a logarithmic term of the form $-(1/2)\log N$ [19]. One might naturally ask how that logarithmic term fits with the terms we find in this manuscript. It turns our that adding a term of the form $(7/6)\log k$, yields the two coefficients that we have established in the 't Hooft limit: $(2/3)\log N$ and $-(7/6)\log\lambda$. In fact all of the numerical results in the 't Hooft limit shown above correspond to the results in the M-theory limit through change of variables $k \to N/\lambda$. The complete correspondence for the special case is

$$\begin{aligned}\mathrm{Re}\log Z(\Delta_a = \pi/2) = &-\frac{\pi\sqrt{2k}}{3}N^{3/2} \\ &+\frac{\pi}{\sqrt{2k}}\left(\frac{k^2}{24}+\frac{1}{3}+1\right)N^{1/2} \\ &-\frac{1}{2}\log N + \frac{7}{6}\log k + \cdots \\ \Rightarrow &-\frac{\pi\sqrt{2}}{3}\frac{N^2}{\sqrt{\lambda}} + \frac{\pi}{24\sqrt{2}}\frac{N^2}{\lambda^{3/2}} + \frac{2}{3}\log N \\ &+\frac{2\pi}{3}\sqrt{2\lambda} - \frac{7}{6}\log\lambda + \cdots,\end{aligned} \tag{3.45}$$

accommodating also the absence of N^2/λ terms discussed previously from the numerical point of view.

IV. DUAL MAGNETICALLY CHARGED ASYMPTOTICALLY ADS$_4$ BLACK HOLES

The low energy gravity dual to the 't Hooft limit of ABJM theory is best described by IIA supergravity on $AdS_4 \times \mathbb{CP}^3$ [1]

$$ds^2_{\text{string}} = \frac{R^3}{k}\left(\frac{1}{4}ds^2(\text{AdS}_4) + ds^2(\mathbb{CP}^3)\right),$$
$$F_4 = \frac{3}{8}R^3\hat{\epsilon}_4, \qquad F_2 = kJ,$$
$$e^{2\phi} = \frac{R^3}{k^3}, \tag{4.1}$$

where $\hat{\epsilon}_4$ is the volume form on AdS_4, J is the Kaehler form on $\mathbb{CP}^3$. This solution is a reduction from 11d supergravity of the Freund-Rubin solution of the form $\text{AdS}_4 \times S^7/\mathbb{Z}_k$ when S^7 is viewed as a $U(1)$ bundle over $\mathbb{CP}^3$. The IIA viewpoint is the appropriate one for large values of k for which the 11d circle would have been very small leading to a breakdown of the 11d supergravity approximation. The radius of curvature in string units is [1]

$$R^2_{\text{str}} = \frac{R^3}{k} = 2^{5/2}\pi\sqrt{\lambda}. \tag{4.2}$$

This expression fits nicely with the field theory expectation that contains in the genus-one term of the topological expansion, that is, in the term of the form N^0, terms of the form $\sqrt{\lambda}$ and also $\log\lambda$. Thus, we expect that, indeed, the logarithmic term might be reproduced by a one-loop supergravity computation of the effective action. Such one-loop corrections are naturally proportional to the logarithm of the overall size.

The above background in Eq. (4.1) corresponds to the vacuum of ABJM theory. To make direct contact with the topologically twisted index we are discussing, one needs to consider more general magnetically charged configurations. Let us start by considering the magnetically charged black hole discussed in [11] which can be embedded into 11d supergravity in the regime where k is a small, fixed, number, $k \sim \mathcal{O}(1)$. The precise embedding equations are given [37]:

$$ds^2_{11} = \Delta^{2/3}ds^2_4 + g^{-2}\Delta^{-1/3}\sum_{i=1}^{4}X_i^{-1}(d\mu_i^2 + \mu_i^2(d\phi_i + gA^{(i)})^2,$$
$$F_4 = 2g\sum_{i=1}^{4}(X_i^2\mu_i^2 - \Delta X_i)\epsilon_{(4)} + \frac{1}{2g}\sum_{i=1}^{4}X_i^{-1}\bar{\star}dX_i \wedge d(\mu_i^2)$$
$$-\frac{1}{2g^2}\sum_{i=1}^{4}X_i^{-2}d(\mu_i^2)\wedge(d\psi_i + gA^i)\wedge\bar{\star}F^i_{(2)},$$
$$\Delta = \sum_{i=1}^{4}X_i\mu_i^2, \tag{4.3}$$

ds^2_4 denotes the four-dimensional metric, X_i are scalar fields and $\sum_{i=1}^4\mu_i^2 = 1$. For more details we refer the reader to [11,37]. We will be very minimalistic and use the properties that we ultimately need. In particular, the key ingredient is a reduction of this solution as to fit in the form of IIA background in Eq. (4.1). The concrete technical problem we need to overcome is that the Ansatz above in Eq. (4.3) is written for a parametrization of the S^7 which is not the $U(1)$ bundle over $\mathbb{CP}^3$ used in Eq. (4.1). Details of the appropriate coordinate changes are worked out in Appendix B. Our main concern is that the seven-dimensional part of the metric background takes the form

$$ds^2_7 = \frac{4}{\Delta^{\frac{1}{3}}}\sum_{i=1}^{4}\frac{1}{X_i}\left(d\mu_i^2 + \mu_i^2\left(d\phi_i + \frac{n_i}{2}\cos\theta d\phi\right)^2\right), \tag{4.4}$$

where we denote the coordinates on S^2 by (θ,ϕ). Given the explicit form of the gauge fields $A_i = (n_i/2)\cos\theta d\phi$ we understand how $\mathbb{CP}^3$ is deformed.

Alternatively, and perhaps more conveniently, we might simply take the four-dimensional point of view. Most of the analysis of the solution was already performed in [11] and rigorous approaches to holographic renormalization of this background were recently presented in [38–40]. The bottom line is that given the prepotential the 4d $\mathcal{N}=2$ gauged supergravity theory, $F = -2i\sqrt{X^0X^1X^2X^3}$ the entropy of the background is simply obtained by

$$S_{\text{BH}} = \frac{2\pi g^2}{G_{4D}}\sqrt{X_1(r_h)X_2(r_h)X_3(r_h)X_4(r_h)}. \tag{4.5}$$

At this point all that is required is that only aspect we need to modify in [11] is the relation between the Newton's constant and the field theory values which can essentially be read off form the background in Eq. (4.1). In the 't Hooft limit we have

$$\frac{2g^2}{G_{4D}} = \frac{2\sqrt{2}}{3}\frac{N^2}{\sqrt{\lambda}}. \tag{4.6}$$

We will not attempt to compute the logarithmic in λ corrections starting from one-loop supergravity in this work. We, however, understand where these corrections might come from and will likely return to this problem in the future.

V. CONCLUSIONS

In this paper we have studied the leading and sub-leading structures of the topologically twisted index of ABJM theory in the 't Hooft limit. We have analytically obtained the leading $N^2/\sqrt{\lambda}$ behavior that matches precisely with the dual Bekenstein-Hawking entropy of magnetically charged asymptotically AdS_4 black holes embedded in IIA string theory on $\text{AdS}_4 \times \mathbb{CP}^3$.

There was probably no doubts in the practitioner's mind that the 't Hooft limit will basically extend the results of the M-theory limit, just as the free energy on S^3 explained the two supergravity scalings [2]; this intuition is rightfully

rooted in the idea of planar dominance on the field theory side. In this paper we have completely clarified the mechanism through which that takes place by presenting various details of the corresponding eigenvalues; in particular, we have clarified the scaling of the eigenvalues changes as we move from one limit to the other.

Beyond the leading scaling with N, that is, the $N^{3/2}$ versus N^2 scaling, important salient differences between the large N, k-fixed limit and the 't Hooft limit show up at sub-leading orders. The quantum expansion of the observables follow widely different patterns and our work here is one first step in the direction of exploring the topologically twisted index in the 't Hooft limit which plays a central role in microscopic counting of the black hole entropy on the dual IIA gravity side. We have explored the topologically twisted index at genus one in the topological expansion. Our results on this part are mostly numerical but the structure constitute important predictions that should be reproduced on the gravitational type IIA string theory side. It would be quite interesting to explore the entropy of the corresponding black holes beyond the leading order and, in particular, to reproduce the $\log(\lambda)$ terms as a quantum one-loop computation in 10d type IIA supergravity.

The topologically twisted index of a certain Chern-Simons matter theory with $SU(N)$ gauge group at level k has recently been matched with the corresponding black hole entropy in massive IIA gravity [15,16] elaborating on previous work [41–43]. More recently, the topologically twisted index has been explored beyond the leading order in N and the coefficient of the logarithm in N term has been determined [20]. It would be interesting to extend the analysis in that case to cover the 't Hooft limit. We have, however, indicated why a logarithmic in λ term is very subleading in the topological expansion as it appears already as a subleading term in the N^0 part of the twisted partition function which is, itself, subleading to the $N^2/\sqrt{\lambda}$ term. We have, nevertheless, presented some very explicit results in the special case where all the fugacities are the same, thus numerically confirming a similar structure in the genus-one term in the topological expansion of the free energy on S^3 and the topologically twisted index treated here.

It would be interesting to discuss more generic field theories using the methods displayed in this manuscript and in [19,20]. It is tantalizing to surmise the existence of certain universality at the subleading order. For the topologically twisted index in the large N, k–fixed limit, we hope to show that there is certain universality in the coefficient of $\log N$ in various classes of theories. The universality of the coefficient of the logarithm of N for the free energy on S^3 for a large class of 3d field theories was established in [44,45] as a consequence of properties of the Airy function. This field theoretic universality of the logarithmic in N term has been reproduced on the gravity side in the M-theory limit in [36] where it is the result of certain topological properties of seven-dimensional manifolds on which the dual eleven-dimensional supergravity is compactified. We anticipate that a similar phenomenon might be present for the topologically twisted indices based on direct numerical analysis and further by arguments of the supergravity description, we will report our findings in an upcoming publication. Armed with these results in the large N, k-fixed limit it seems likely that the 't Hooft limit will also lead to a certain universality in the subleading terms of the $1/N$ expansion. However, given the structure of the topological expansion the potential logarithmic term turns out to be logarithmic in λ and becomes technically harder to extract.

On the more speculative side it would be quite interesting to explore whether the topological expansion of the index follows the free energy on S^3 in the sense that the coefficients of the topological expansion $\log Z = \sum g_s^{2g-2} F_g$ lead to F_g with interesting modular properties. Such structure might not only clarify conceptually the nature of the expansion but will also provide an analytic understanding of the growth in the number of degrees of freedom setting up further high precision comparison with the gravitational side.

ACKNOWLEDGMENTS

We are thankful to F. Benini, A. Faraggi, F. Ferrari, A. González Lezcano, L. Griguolo, J. Hong, J. T. Liu, J. F. Morales, K. Okuyama, P. Putrov, I. Yaakov and A. Zaffaroni for comments. This work is partially supported by the U.S. Department of Energy under Grant No. DE-SC0007859.

APPENDIX A: ALGORITHMIC DETAILS

Let us discuss various technical details regarding the numerical algorithms for solving the Bethe Ansatz equations. A flow chart of the main algorithm is illustrated in table V. We use $\{u_i^I, \tilde{u}_j^I\}$ to represent the starting point and $\{u_i^E, \tilde{u}_j^E\}$ to represent the exact solution of the

TABLE V. The flow chart of the iterative algorithm for solving the BAE.

$\{u_i, \tilde{u}_j\}$	N_o	$\cdots$	N_n	N_{n+1}	$\cdots$	N_f
k_o	$\{u_i, \tilde{u}_j\}^{(o)}$	$\rightarrow$	$\{u_i, \tilde{u}_j\}^{(n)}$	$\{u_i, \tilde{u}_j\}^{(n+1)}$	$\rightarrow$	
$\vdots$	$\downarrow$					
k_m	$\{u_i, \tilde{u}_j\}^{(m)}$					
k_{m+1}	$\{u_i, \tilde{u}_j\}^{(m+1)}$					
$\vdots$	$\downarrow$					
k_f						$\{u_i, \tilde{u}_j\}^{(f)}$

variables $\{u_i, \tilde{u}_j\}$. The starting point $\{u_i^I, \tilde{u}_j^I\}^{(o)}$ of the whole algorithm is the leading order eigenvalue distribution obtained in [11] and the exact solution $\{u_i^E, \tilde{u}_j^E\}^{(o)}$ to the BAE with $k = 1$ and small N (for example, $N = 50$) can be obtained using FindRoot in *Mathematica* as implemented in [19]. Because assigning a value to k is equivalent to assigning a value to $\lambda(= N/k)$, we will use k to illustrate the numerical algorithm in the following.

The iterative algorithm contains two parts. The first part is for the BAE with a fixed N but different values of k, namely the vertical direction. The solutions in the same column have the same dimension $2N$. The behavior of the eigenvalues in Eq. (3.3) implies an iterative relation

$$\begin{aligned}\{u_i^I, \tilde{u}_j^I\}^{(m+1)} &= i\sqrt{\frac{k_m}{k_{m+1}}}\mathrm{Im}(\{u_i^E, \tilde{u}_j^E\}^{(m)}) + \mathrm{Re}(\{u_i^E, \tilde{u}_j^E\}^{(m)}) - \frac{\pi}{k_m} + \frac{\pi}{k_{m+1}},\\ \{u_i^E, \tilde{u}_j^E\}^{(m+1)} &= \mathrm{FindRoot}[\mathrm{BAE}(N_o, k_{m+1}), \{u_i^I, \tilde{u}_j^I\}^{(m+1)}].\end{aligned} \tag{A1}$$

Thus the first iterative algorithm is k iterative algorithm (Algorithm 1). It is worth noting that the number of the step N_{ks} for iterating over k can be set to 1 for the special case, but has to satisfy the condition $k_s = (k_f/k_o)^{1/N_{ks}} \gtrapprox 1$ for the general cases.

Algorithm 1: k iterative algorithm.

Input: $N_o, k_o, \{u_i^E, \tilde{u}_j^E\}^{(o)}, k_f, N_{ks}$;
Initialize $\{u_i^E, \tilde{u}_j^E\} = \{u_i^E, \tilde{u}_j^E\}^{(o)}; k_s = (k_f/k_o)^{1/N_{ks}}$;
for $k = k_o \times k_s, k_o \times k_s^2, \cdots,$ **to** $k = k_f$ **do**
  $\{u_i^I, \tilde{u}_j^I\} := i\sqrt{1/k_s}\mathrm{Im}\left(\{u_i^E, \tilde{u}_j^E\}\right) + \mathrm{Re}\left(\{u_i^E, \tilde{u}_j^E\}\right) - \pi/(k/k_s) + \pi/k$;
  $\{u_i^E, \tilde{u}_j^E\} := \mathrm{FindRoot}\left[\mathrm{BAE}(N_o, k), \{u_i^I, \tilde{u}_j^I\}\right]$;

The second part is for the BAE with a fixed k but different values of N, namely the horizontal direction. Because the dimension of the solutions in the same row is dependent on N, the method of interpolation should be used in this iterative algorithm. Also implied by the behavior form in Eq. (3.3), the iterative relation is

$$\begin{aligned}t^{(n)}(i) &= \mathrm{Interpolation}\left[\left\{\frac{i-1}{N_n - 1}, \sqrt{\frac{k_o}{N_n}}\mathrm{Im}((u_i^E)^{(n)})\right\}, \quad i = 1, 2, \ldots, N_n\right],\\ dv^{(n)}(i) &= \mathrm{Interpolation}\left[\left\{\frac{i-1}{N_n - 1}, -2\left(\mathrm{Re}((u_i^E)^{(n)}) - \frac{\pi}{k_o}\right)\right\}, \quad i = 1, 2, \ldots, N_n\right],\\ (u_i^I)^{(n+1)} &= i\sqrt{\frac{N_{n+1}}{k_o}}t^{(n)}\left(\frac{i-1}{N_{n+1}-1}\right) + \frac{\pi}{k_o} - \frac{1}{2}dv^{(n)}\left(\frac{i-1}{N_{n+1}-1}\right), \quad i = 1, 2, \ldots, N_{n+1},\\ (\tilde{u}_j^I)^{(n+1)} &= i\sqrt{\frac{N_{n+1}}{k_o}}t^{(n)}\left(\frac{j-1}{N_{n+1}-1}\right) + \frac{\pi}{k_o} + \frac{1}{2}dv^{(n)}\left(\frac{j-1}{N_{n+1}-1}\right), \quad j = 1, 2, \ldots, N_{n+1},\\ \{u_i^E, \tilde{u}_j^E\}^{(n+1)} &= \mathrm{FindRoot}[\mathrm{BAE}(N_{n+1}, k_o), \{u_i^I, \tilde{u}_j^I\}^{(n+1)}].\end{aligned} \tag{A2}$$

Thus the second iterative algorithm is N iterative algorithm (Algorithm 2). It is worth noting that the step N_s for iterating over N is a natural number and much less than $N(N \sim 100)$. In the line $(*)$ of the algorithm, $k := k_o$ is for the M-theory limit. Since N changes smoothly, we can set $k := (N/N_o)k_o$ for the 't Hooft limit.

Algorithm 2: N iterative algorithm.

Input: $N_o, k_o, \{u_i^E, \tilde{u}_j^E\}^{(o)}, N_f, N_s$;
Initialize $\{u_i^E, \tilde{u}_j^E\} = \{u_i^E, \tilde{u}_j^E\}^{(o)}; N_I = N_o; k_I = k_o$;
for $N = N_o + N_s, N_o + 2N_s, \cdots,$ **to** $N = N_f$ **do**
  $t(i) := \text{Interpolation}\left[\left\{\frac{i-1}{N_I-1}, \sqrt{\frac{k_I}{N_I}}\text{Im}\left(u_i^E\right)\right\}, i = 1, 2, \cdots, N_I\right]$;
  $dv(i) := \text{Interpolation}\left[\left\{\frac{i-1}{N_I-1}, -2\left(\text{Re}\left(u_i^E\right) - \frac{\pi}{k_I}\right)\right\}, i = 1, 2, \cdots, N_I\right]$;
  $k := k_o$; // $(*)$ $k := (N/N_o)k_o$;
  for $i = 1 : N$ **do**
    $u_i^I := i\sqrt{\frac{N}{k}}t\left(\frac{i-1}{N-1}\right) + \frac{\pi}{k} - \frac{1}{2}dv\left(\frac{i-1}{N-1}\right)$;
    $\tilde{u}_i^I := i\sqrt{\frac{N}{k}}t\left(\frac{i-1}{N-1}\right) + \frac{\pi}{k} + \frac{1}{2}dv\left(\frac{i-1}{N-1}\right)$;
  $N_I := N; k_I := k$;
  $\{u_i^E, \tilde{u}_j^E\} := \text{FindRoot}\left[\text{BAE}(N, k), \{u_i^I, \tilde{u}_j^I\}\right]$;

Theoretically, the BAE with any values of N and k can be solved using the combination of the k iterative algorithm and N iterative algorithm. However, with increasing N, the scale and complexity of the BAE increases so that it takes much more time to arrive at the final solution, especially for the cases with general fugacities. Therefore, we choose to obtain the numerical solutions up to $N = 300$–400. As an example, the detailed information of the numerical computation in Table I is shown in Table VI. WP means WorkingPrecision in *Mathematica*, BAE time means the time of solving the BAE and Re log Z time means the time of calculating the index.

APPENDIX B: PARAMETRIZATIONS OF S^7

In this appendix we describe the embedding of magnetically charged asymptotically AdS_4 black holes, such as those of [46] in eleven and ten-dimensional contexts. We first discuss the setup of [37] paying particular attention to the details of the reduction to 10d. Let us write S^7 as a $U(1)$ bundle over $\mathbb{CP}^3$

$$ds^2_{S^7} = \frac{1}{16}(d\zeta + A)^2 + \frac{1}{4}\Big[d\alpha^2 + \cos^2\frac{\alpha}{2}(d\theta_1^2 + \sin^2\theta_1^2 d\varphi_1^2) + \sin^2\frac{\alpha}{2}(d\theta_2^2 + \sin^2\theta_2^2 d\varphi_2^2) + \sin^2\frac{\alpha}{2}\cos^2\frac{\alpha}{2}(d\chi + \cos\theta_1 d\varphi_1 - \cos\theta_2 d\varphi_2)\Big], \tag{B1}$$

where

$$A = \cos\alpha d\chi + 2\cos^2\frac{\alpha}{2}\cos\theta_1 d\varphi_1 + 2\sin^2\frac{\alpha}{2}\cos\theta_2 d\varphi_2.$$

The above metric can be reached by considering [47]

TABLE VI. The information of the numerical computation in Table I.

Δ_a	λ	k_o	N_o	N range	N_{ks}	N_s	WP	BAE time	Re log Z time
Special	1, 5, 10	1	100	100–300	1	10	200	2 hrs	40 min
General	1	1	50	50–300	10	5	600	33 hrs	3 hrs 40 min
	5	1	50	50–300	10	10	300	10 hrs	3 hrs 22 min
	10	1	50	50–300	10	10	300	10 hrs	3 hrs 30 min

$$z_1 = \cos\frac{\alpha}{2}\cos\frac{\theta_1}{2}\exp[i(2\varphi_1+\chi+\zeta)/4],$$
$$z_2 = \cos\frac{\alpha}{2}\sin\frac{\theta_1}{2}\exp[i(-2\varphi_1+\chi+\zeta)/4],$$
$$z_3 = \cos\frac{\alpha}{2}\cos\frac{\theta_2}{2}\exp[i(2\varphi_2-\chi+\zeta)/4],$$
$$z_4 = \cos\frac{\alpha}{2}\sin\frac{\theta_2}{2}\exp[i(-2\varphi_2-\chi+\zeta)/4], \tag{B2}$$

which satisfy $\sum_{i=1}^{4}|z_i|^2 = 1$.

We have different options for writing S^7 as foliations of spheres,

$$ds^2_{S^7} = \sum_{i=1}^{4}(d\mu_i^2 + \mu_i^2 d\phi_i^2). \tag{B3}$$

For example, taking

$$\mu_1 = \sin\theta,$$
$$\mu_2 = \cos\theta\sin\varphi,$$
$$\mu_2 = \cos\theta\cos\varphi\sin\psi,$$
$$\mu_4 = \cos\theta\cos\varphi\cos\psi \tag{B4}$$

leads to

$$ds^2_{S^7} = d\theta^2 + \sin^2\theta d\phi_1^2 + \cos^2\theta(d\varphi^2 + \cos^2\varphi(d\psi^2 + \sin^2\psi d\phi_3^2 + \cos^2\psi d\phi_4^2) + \sin^2\varphi d\phi_2^2), \tag{B5}$$

which is a foliation of $S^5 \times S^1$. For a foliation of S^7 over $S^3 \times S^3$ we need:

$$\mu_1 = \cos\frac{\alpha}{2}\cos\frac{\theta_1}{2}$$
$$\mu_2 = \sin\frac{\alpha}{2}\sin\frac{\theta_1}{2},$$
$$\mu_2 = \cos\frac{\alpha}{2}\cos\frac{\theta_2}{2},$$
$$\mu_4 = \sin\frac{\alpha}{2}\sin\frac{\theta_2}{2}, \tag{B6}$$

which leads to

$$ds^2_{S^7} = d\alpha^2 + \cos^2\alpha(d\theta_1^2 + \cos^2\theta_1 d\phi_1^2 + \sin^2\theta_1 d\phi_2^2) + \sin^2\alpha(d\theta_2^2 + \cos^2\theta_2 d\phi_3^2 + \sin^2\theta_2 d\phi_4^2). \tag{B7}$$

It becomes clear in either of these parametrizations that the fiber in ζ is obtained as the sum of the angles ϕ_i in the (μ_i, ϕ_i) parametrization.

$$\zeta = \frac{1}{4}(\phi_1 + \phi_2 + \phi_3 + \phi_4). \tag{B8}$$

This is the angle for which, upon reduction to ten dimensions one recovers the background in Eq. (4.1) in the absences of charges and for trivial scalar fields.

[1] O. Aharony, O. Bergman, D. L. Jafferis, and J. Maldacena, $\mathcal{N}=6$ superconformal Chern-Simons-matter theories, M2-branes and their gravity duals, J. High Energy Phys. 10 (2008) 091.

[2] N. Drukker, M. Marino, and P. Putrov, From weak to strong coupling in ABJM theory, Commun. Math. Phys. **306**, 511 (2011).

[3] N. Drukker, M. Marino, and P. Putrov, Nonperturbative aspects of ABJM theory, J. High Energy Phys. 11 (2011) 141.

[4] F. Benini and A. Zaffaroni, A topologically twisted index for three-dimensional supersymmetric theories, J. High Energy Phys. 07 (2015) 127.

[5] M. Honda and Y. Yoshida, Supersymmetric index on $T^2 \times S^2$ and elliptic genus, arXiv:1504.04355.

[6] C. Closset, S. Cremonesi, and D. S. Park, The equivariant A-twist and gauged linear sigma models on the two-sphere, J. High Energy Phys. 06 (2015) 076.

[7] F. Benini and A. Zaffaroni, Supersymmetric partition functions on Riemann surfaces, Proc. Symp. Pure Math. **96**, 13 (2017).

[8] C. Closset and H. Kim, Comments on twisted indices in 3d supersymmetric gauge theories, J. High Energy Phys. 08 (2016) 059.

[9] C. Closset, H. Kim, and B. Willett, Supersymmetric partition functions and the three-dimensional A-twist, J. High Energy Phys. 03 (2017) 074.

[10] C. Closset, H. Kim, and B. Willett, Seifert fibering operators in 3d $\mathcal{N}=2$ theories, J. High Energy Phys. 08 (2016) 059.

[11] F. Benini, K. Hristov, and A. Zaffaroni, Black hole microstates in AdS_4 from supersymmetric localization, J. High Energy Phys. 05 (2016) 054.

[12] F. Benini, K. Hristov, and A. Zaffaroni, Exact microstate counting for dyonic black holes in AdS_4, Phys. Lett. B **771**, 462 (2017).

[13] A. Cabo-Bizet, V. I. Giraldo-Rivera, and L. A. Pando Zayas, Microstate counting of AdS_4 hyperbolic black hole entropy via the topologically twisted index, J. High Energy Phys. 08 (2017) 023.

[14] F. Azzurli, N. Bobev, P. M. Crichigno, V. S. Min, and A. Zaffaroni, A universal counting of black hole microstates in AdS_4, J. High Energy Phys. 02 (2018) 054.

[15] S. M. Hosseini, K. Hristov, and A. Passias, Holographic microstate counting for AdS_4 black holes in massive IIA supergravity, J. High Energy Phys. 10 (2017) 190.
[16] F. Benini, H. Khachatryan, and P. Milan, Black hole entropy in massive Type IIA, Classical Quantum Gravity **35**, 035004 (2018).
[17] S. M. Hosseini, Black hole microstates and supersymmetric localization, Ph.D. thesis, Milan Bicocca University, 2018.
[18] A. Zaffaroni, Lectures on AdS black holes, holography and localization, arXiv:1902.07176.
[19] J. T. Liu, L. A. Pando Zayas, V. Rathee, and W. Zhao, Toward microstate counting beyond large N in localization and the dual one-loop quantum supergravity, J. High Energy Phys. 01 (2018) 026.
[20] J. T. Liu, L. A. Pando Zayas, and S. Zhou, Subleading microstate counting in the dual to massive Type IIA, arXiv:1808.10445 [Phys. Rev. D (to be published)].
[21] J. T. Liu, L. A. Pando Zayas, V. Rathee, and W. Zhao, One-Loop Test of Quantum Black Holes in Anti–de Sitter Space, Phys. Rev. Lett. **120**, 221602 (2018).
[22] I. Jeon and S. Lal, Logarithmic corrections to entropy of magnetically charged AdS_4 black holes, Phys. Lett. B **774**, 41 (2017).
[23] K. Hristov, I. Lodato, and V. Reys, On the quantum entropy function in 4d gauged supergravity, J. High Energy Phys. 07 (2018) 072.
[24] D. Gang and N. Kim, Large N twisted partition functions in 3d-3d correspondence and holography, Phys. Rev. D **99**, 021901 (2019).
[25] D. Gang, N. Kim, and L. A. Pando Zayas, Precision microstate counting for the entropy of wrapped M5-branes, arXiv:1905.01559.
[26] C. P. Herzog, I. R. Klebanov, S. S. Pufu, and T. Tesileanu, Multi-matrix models and tri-Sasaki Einstein spaces, Phys. Rev. D **83**, 046001 (2011).
[27] S. M. Hosseini and A. Zaffaroni, Large N matrix models for 3d $\mathcal{N}=2$ theories: Twisted index, free energy and black holes, J. High Energy Phys. 08 (2016) 064.
[28] S. M. Hosseini and N. Mekareeya, Large N topologically twisted index: Necklace quivers, dualities, and Sasaki-Einstein spaces, J. High Energy Phys. 08 (2016) 089.
[29] M. Marino and P. Putrov, Exact results in ABJM theory from topological strings, J. High Energy Phys. 06 (2010) 011.
[30] H. Ooguri and C. Vafa, World sheet derivation of a large N duality, Nucl. Phys. **B641**, 3 (2002).
[31] K. Okuyama, Instanton corrections of 1/6 BPS Wilson loops in ABJM theory, J. High Energy Phys. 09 (2016) 125.
[32] J. T. Liu and R. Minasian, Computing $1/N^2$ corrections in AdS/CFT, arXiv:1010.6074.
[33] A. Sen, Logarithmic corrections to $\mathcal{N}=2$ black hole entropy: An infrared window into the microstates, Gen. Relativ. Gravit. **44**, 1207 (2012).
[34] A. Sen, Logarithmic corrections to rotating extremal black hole entropy in four and five dimensions, Gen. Relativ. Gravit. **44**, 1947 (2012).
[35] A. Sen, Microscopic and macroscopic entropy of extremal black holes in string theory, Gen. Relativ. Gravit. **46**, 1711 (2014).
[36] S. Bhattacharyya, A. Grassi, M. Marino, and A. Sen, A one-loop test of quantum supergravity, Classical Quantum Gravity **31**, 015012 (2014).
[37] M. Cvetic, M. J. Duff, P. Hoxha, J. T. Liu, H. Lu, J. X. LuR. Martinez-Acosta, C. N. Pope, H. Sati, and T. A. Tran, Embedding AdS black holes in ten-dimensions and eleven-dimensions, Nucl. Phys. **B558**, 96 (1999).
[38] N. Halmagyi and S. Lal, On the on-shell: The action of AdS_4 black holes, J. High Energy Phys. 03 (2018) 146.
[39] A. Cabo-Bizet, U. Kol, L. A. Pando Zayas, I. Papadimitriou, and V. Rathee, Entropy functional and the holographic attractor mechanism, J. High Energy Phys. 05 (2018) 155.
[40] P. Benetti Genolini, J. M. Pérez Ipiña, and J. Sparks, Localization of the action in AdS/CFT, J. High Energy Phys. 10 (2019) 252.
[41] A. Guarino and J. Tarrio, BPS black holes from massive IIA on S^6, J. High Energy Phys. 09 (2017) 141.
[42] A. Guarino, D. L. Jafferis, and O. Varela, String Theory Origin of Dyonic $\mathcal{N}=8$ Supergravity and its Chern-Simons Duals, Phys. Rev. Lett. **115**, 091601 (2015).
[43] O. Varela, AdS_4 solutions of massive IIA from dyonic ISO (7) supergravity, J. High Energy Phys. 03 (2016) 071.
[44] M. Marino and P. Putrov, ABJM theory as a Fermi gas, J. Stat. Mech. (2012) P03001.
[45] H. Fuji, S. Hirano, and S. Moriyama, Summing up all genus free energy of ABJM matrix model, J. High Energy Phys. 08 (2011) 001.
[46] S. L. Cacciatori and D. Klemm, Supersymmetric AdS_4 black holes and attractors, J. High Energy Phys. 01 (2010) 085.
[47] M. Cvetic, H. Lu, and C. N. Pope, Consistent warped space Kaluza-Klein reductions, half maximal gauged supergravities and CP^n constructions, Nucl. Phys. **B597**, 172 (2001).